npj | parkinson's disease

Article

Published in partnership with the Parkinson's Foundation

https://doi.org/10.1038/s41531-025-01006-y

EGFR phosphorylates DNAJB1 to suppress α-synuclein aggregation in Parkinson's disease

Yun-Yu Huang[1,2], Sue-Jane Lin[1], Wei-Yu Chiang[1], Yuan-Teng Chang[1,3], Chan-Chih Yang[1], Chia-Yu Liao[1], Ya-Lan Chang[1], Chin-Hsien Lin[2] ✉ & Shu-Chun Teng[1] ✉

Parkinson's disease (PD), characterized by α-synuclein accumulation in dopaminergic neurons, is a common neurodegenerative disorder. Recent findings highlight DNAJB1 as a crucial factor in the disaggregation of α-synuclein fibrils in vitro, yet the underlying mechanisms and regulatory processes in neuronal cells remain largely undefined. This study reveals that DNAJB1 facilitates the clearance of α-synuclein via the Hsp70 chaperone system. Phosphorylation of DNAJB1 at tyrosine 5 by the epidermal growth factor receptor (EGFR) is essential for mitigating α-synuclein aggregation, enhancing its interaction with Hsp70. Dysregulation of this pathway disrupts α-synuclein delivery to Hsp70, worsening aggregation in neuronal cells. Analysis of human brain lysates from individuals with PD and unaffected controls showed reduced levels of EGFR and DNAJB1, with an increase in phosphorylated DNAJB1 at Y5. These findings elucidate mechanisms in PD pathology and suggest DNAJB1 as a promising candidate for targeted therapeutic strategies.

PD is a common neurodegenerative disease characterized by distinct motor symptoms such as tremors, rigidity, and bradykinesia[1]. The pathognomonic features of PD involve the progressive death of dopaminergic neurons, particularly in the substantia nigra[2]. Abnormal accumulation of misfolded α-synuclein in their cytoplasm causes the formation of Lewy bodies and promotes neurodegeneration[3]. However, the precise cause of PD is not completely understood, but it probably results from the mix of genetic mutations and environmental factors triggering α-synuclein misfolding and aggregation[4].

The accumulation of misfolded or aggregated proteins leading to the collapse in proteostasis is a common feature of aging[5,6]. Chaperones specifically participate in the process of protein folding and fulfill a significant function in the folding system under stress conditions. Among these chaperones, heat shock protein 70 (Hsp70) is essential for protein folding, functioning through the hydrolysis of ATP and the involvement of cofactors to modulate the cycles of binding and release. This mechanism is crucial for ensuring the correct folding of proteins[7,8]. Furthermore, co-chaperone J-domain proteins (JDPs) play a significant role in identifying specific client proteins and facilitating their delivery to Hsp70.

Moreover, environmental change may alter the folding ability of the chaperone system. Glucose intake triggers the phosphorylation of a co-chaperone, which decreases its binding affinity with Hsp90 and results in the accumulation of misfolded proteins in yeast[9]. Stress-induced phosphorylation of co-chaperones may control the binding affinity not only with the chaperone but also with the clients. Under DNA double strands breaks, DNAJB11 undergoes phosphorylation to increase the binding affinity with α-synuclein to alleviate its aggregation[10]. Therefore, cells can sense environmental changes and control the function of co-chaperones through posttranslational modification.

In the initial step of the folding cycle, specific JDPs identify and bind to distinct cargo molecules, subsequently facilitating their delivery to Hsp70[11]. In humans, there are more than 50 JDPs categorized into three types based on their structures[12]. DNAJB1 was discovered to facilitate Hsc70 in disassembling tau fibrils in vitro[13] and also disaggregates α-synuclein fibrils in vitro[14–17]. Conversely, another study demonstrated that DNAJB6 inhibits the formation of aggregated α-synuclein in non-neuronal HEK293 cells[18]. Additionally, a case report identified a DNAJB2 mutation in a family with Charcot-Marie-Tooth disease type 2, characterized by hearing loss and parkinsonism[19]. Another research discovered a large *DNAJB2* deletion in a family with spinal muscular atrophy and parkinsonism[20]. Given that these findings have not been experimentally validated in neuronal cells, the central

[1]Department of Microbiology, College of Medicine, National Taiwan University, Taipei, Taiwan. [2]Department of Neurology, National Taiwan University Hospital Taipei, Taipei, Taiwan. [3]Department of Physiology and Pharmacology, College of Veterinary Medicine, University of Georgia, Athens, Georgia, USA. ✉e-mail: chlin@ntu.edu.tw; shuchunteng@ntu.edu.tw

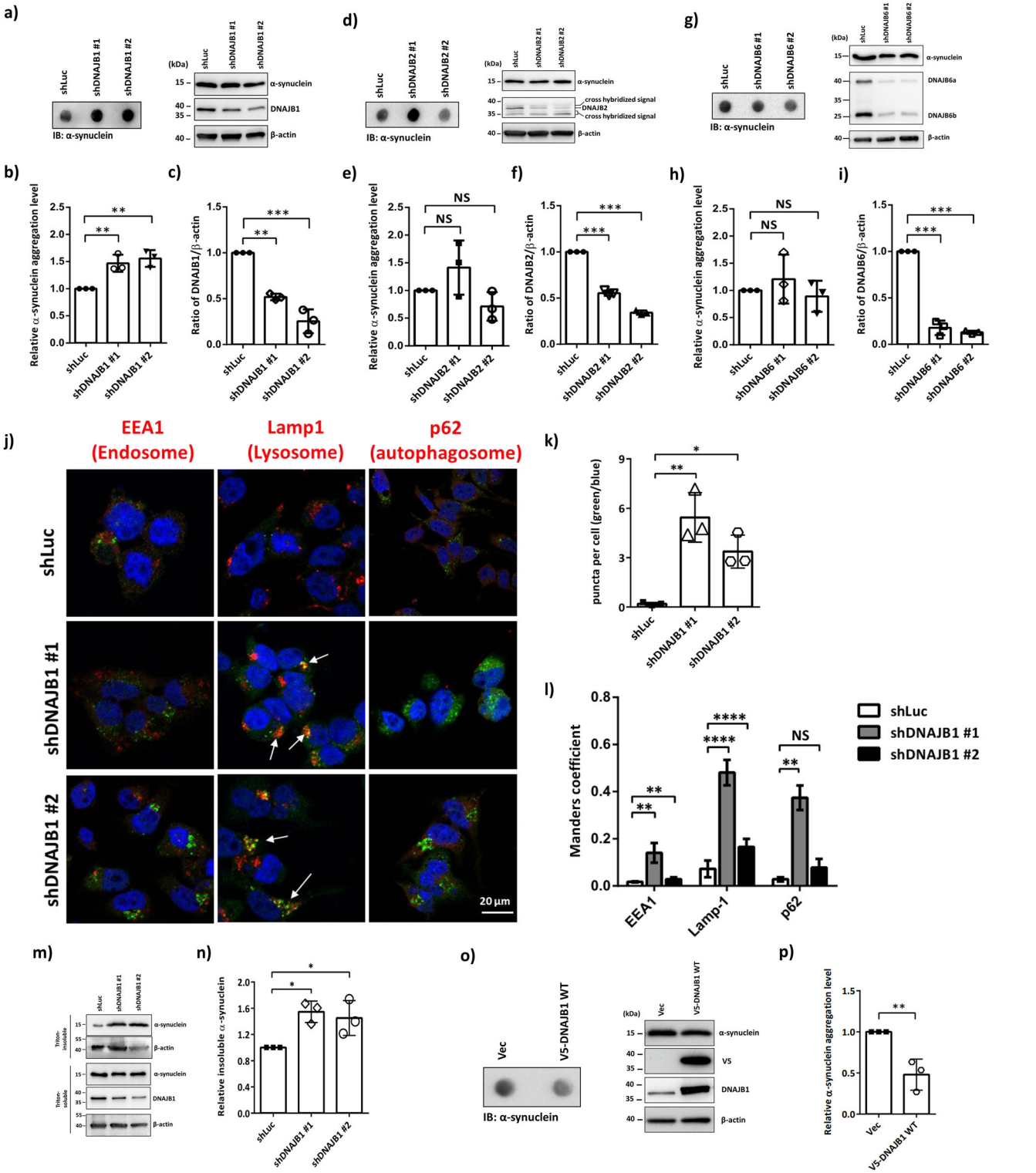

factor responsible for recruiting α-synuclein to the Hsp70 system for disaggregation in neuronal cells remains unclear.

Numerous studies revealed decreased levels of EGFR in the cerebrospinal fluid, blood, or specific brain regions of individuals with PD[21–23]. Furthermore, clinical investigations identified a correlation between *EGFR* variations and susceptibility to the risk of PD[24]. With these reports supporting the link between EGFR and PD, EGFR has emerged as a potential biomarker or risk genetic factor contributing to the disease[24]. These findings imply that EGFR may play a pivotal role in maintaining α-synuclein homeostasis, a key protein involved in PD pathology. However, the precise mechanism through which EGFR preserves the folding and stability of α-synuclein remains elusive, representing a significant unresolved puzzle in the field of PD research. Here, we explore the EGFR-mediated regulation of the JDP specific for α-synuclein and understand how the phosphorylation of DNAJB1 by EGFR facilitates the folding of α-synuclein.

Fig. 1 | DNAJB1 decreases α-synuclein aggregates. a Chemiluminescence images of α-synuclein, DNAJB1, and β-actin. SH-SY5Y cells expressing shLuc and shDNAJB1 were pretreated with 100 nM rotenone for 24 h, followed by the analysis of α-synuclein aggregation via filter trap assay. Data were analyzed by one-way ANOVA with Dunnett's test. **b** Quantification of aggregation levels normalized to β-actin in shDNAJB1 SH-SY5Y cells. **c** The knockdown efficiency of DNAJB1. **d** Chemiluminescence images of α-synuclein, DNAJB2, and β-actin. **e** Quantification of aggregation levels normalized to β-actin in shDNAJB2 SH-SY5Y cells. **f** The knockdown efficiency of DNAJB2. **g** Chemiluminescence images of α-synuclein, DNAJB6, and β-actin. **h** Quantification of aggregation levels normalized to β-actin in shDNAJB6 SH-SY5Y cells. **i** The knockdown efficiency of DNAJB6. **j** After 24 h pretreatment with 100 nM rotenone, shDNAJB1 SH-SY5Y cells were fixed and stained with indicated antibodies (α-synuclein in green, each organelle marker in red) and counter-stained with DAPI to stain the nucleus (blue). All fluorescence images were captured using a Zeiss LSM780 confocal fluorescence microscope. Scale bar: 20 μm. **k** The numbers of puncta in the cells were quantified from 5 fields. Data was analyzed by one-way ANOVA with Dunnett's test. **l** Colocalization analysis between α-synuclein (green) and each organelle (red) from 5 fields. Data was analyzed by two-way ANOVA with Dunnett's test. **m** shDNAJB1 SH-SY5Y cells were harvested after 24 h rotenone treatment. The cell lysates were biochemically fractionated into Triton-soluble and -insoluble fractions as described in "Methods". The DNAJB1 expression levels, and Triton-soluble and -insoluble fractions of α-synuclein were analyzed by western blotting. The β-actin was used as a loading control. **n** Quantification of the Triton-insoluble form of α-synuclein shown in (**m**). The Triton-insoluble form of α-synuclein was normalized to β-actin. Data was analyzed by one-way ANOVA with Dunnett's test. **o** A representative image of the filter trap assay showed that overexpression of DNAJB1 significantly reduced α-synuclein aggregation in SH-SY5Y cells. **p** Data was analyzed with unpaired two-tailed Student's t-test. Each dataset is expressed as mean ± SD for $n = 3$. $^{*}P < 0.05$, $^{**}P < 0.01$, $^{***}P < 0.001$, $^{****}P < 0.0001$.

Results

DNAJB1 decreases α-synuclein aggregates in human neuroblastoma cells

To elucidate α-synuclein aggregation in PD, we screened JDPs for their potential to resolve these aggregates in neuronal cells. Using a filter-trap assay that has been used to detect protein aggregation in human neuroblastoma cell lines[25–28], we assessed three JDPs previously linked to α-synuclein aggregation[16–20]. As shown in Fig. 1a–i, only DNAJB1, but not DNAJB2 or DNAJB6, resolves α-synuclein aggregation in human neuroblastoma SH-SY5Y cells. The knockdown efficiency was analyzed at the protein level by western blotting (Fig. 1c, f, i). We observed an incomplete knockdown, which may suggest that the JDPs play critical roles. Quantitative reverse transcription PCR (qRT-PCR) was used to analyze whether DNAJB1 knockdown changes in the mRNA level of SNCA. As shown in Fig. S1a, the knockdown of DNAJB1 does not alter the mRNA level of *SNCA*.

To further confirm whether DNAJB1 resolves α-synuclein aggregation in SH-SY5Y cells, confocal microscopy was employed to observe the formation of aggregated puncta[10]. Compared to the knockdown of firefly luciferase (shLuc) control cells, an increased presence of α-synuclein aggregates was observed, suggesting an enhanced level of α-synuclein aggregation within the cells (Fig. 1j, k). DNAJB1 knockdown causes these α-synuclein aggregates to localize primarily in endosomal and lysosomal compartments, with a more substantial accumulation observed in the lysosome relative to the endosome (Fig. 1j, l). Furthermore, cell fractionation analysis reveals that knockdown of DNAJB1 results in an elevated insoluble fraction of α-synuclein (Fig. 1m, n)[29].

The *GBA1* gene encodes the lysosomal enzyme β-glucocerebrosidase (GCase), which facilitates the hydrolysis of glucosylceramide (GlcCer) into ceramide and glucose[30]. Heterozygous mutations in *GBA1* constitute the most prevalent genetic risk factor for PD[31]. Several prior studies have indicated alterations in both the expression levels and subcellular localization of GBA in PD models[32,33]. To investigate whether the increased α-synuclein protein aggregation was caused by alteration of the levels of heat shock proteins and GBA, the protein levels of a subset of HSP70s (HSPA8 and HSPA1A) and GBA were detected by western blotting in shLuc and shDNAJB1 SH-SY5Y cells. Knockdown of DNAJB1 does not change the protein levels of these Hsp70 molecular chaperones and GBA (Fig. S1b–f). As shown in Fig. S1g, h, knockdown of DNAJB1 does not induce colocalization of GBA with endosomes, lysosomes, or autophagosomes. Nevertheless, overexpression of DNAJB1 reduces α-synuclein aggregation (Fig. 1o, p). The findings from the filter trap assay, the accumulation of aggregated α-synuclein puncta, and cell fractionation analysis all exhibit the important role of DNAJB1. These results suggest that DNAJB1 may deliver α-synuclein to the Hsp70 folding system to reduce α-synuclein aggregation in human neuroblastoma cells.

Table 1 | The phosphorylation sites on DNAJB1 were reported in the PhosphoSitePlus database (https://www.phosphosite.org/proteinAction.action?id=13798&showAllSites=true)

Site	Amino acids sequence of DNAJB1	LTP*	HTP**
Y5	___MGkDyYQTLGLA	0	5
S16	LGLArGAsDEEIkRA	0	2
Y52	FkEIAEAyDVLSDPR	0	1
T88	SGGGANGtsFSYTFH	0	1
S89	GGGANGtsFSYTFHG	0	1
S149	TNVNFGRsRsAQEPA	1	0
S151	VNFGRsRsAQEPARK	1	2
S171	VTHDLRVsLEElysG	1	2
Y176	RVsLEElysGCtkKM	0	506
S177	VsLEElysGCtkKMK	0	3
T180	EElysGCtkKMKIsH	0	1
S186	CtkKMKIsHKRLNPD	0	4
S196	RLNPDGksIRNEDkI	0	2
T205	RNEDkILtIEVKKGW	0	2
T227	FPkEGDQtsNNIPAD	0	1
S228	PkEGDQtsNNIPADI	0	1
S252	NIFkRDGsDVIyPAR	0	2
Y256	RDGsDVIyPARIsLR	0	1
S261	VIyPARIsLREALCG	0	1
T307	EGLPLPktPEKRGDL	0	11

*Low throughput papers (LTP): The number of records in which this modification site was determined using other than discovery mass spectrometry.
**High throughput papers (HTP): The number of records in which this modification site was assigned only using proteomic mass spectrometry.

DNAJB1 tyrosine 5 phosphorylation is crucial for resolving α-synuclein aggregation

To acquire insights into how DNAJB1 clears α-synuclein aggregation under stress, we examined the regulation of DNAJB1 in neuronal cells. Previous studies reported that phosphorylation can be a key regulation in controlling proteostasis during the aging process or upon double-strand breaks[9,10]. We, therefore, focused on whether phosphorylation controls regulations between DNAJB1 and α-synuclein. In the PhosphoSitePlus database, tyrosine 5, tyrosine 176, and threonine 307 of DNAJB1 were reported to be phosphorylated from over 5 high-throughput reports (Table 1). We mutated these three phosphorylation sites to dephosphor-mimicking alanine/phenylalanine (A/F) and phosphor-mimicking aspartic/glutamic acid (D/E) to see whether these mutations change their folding ability to clients

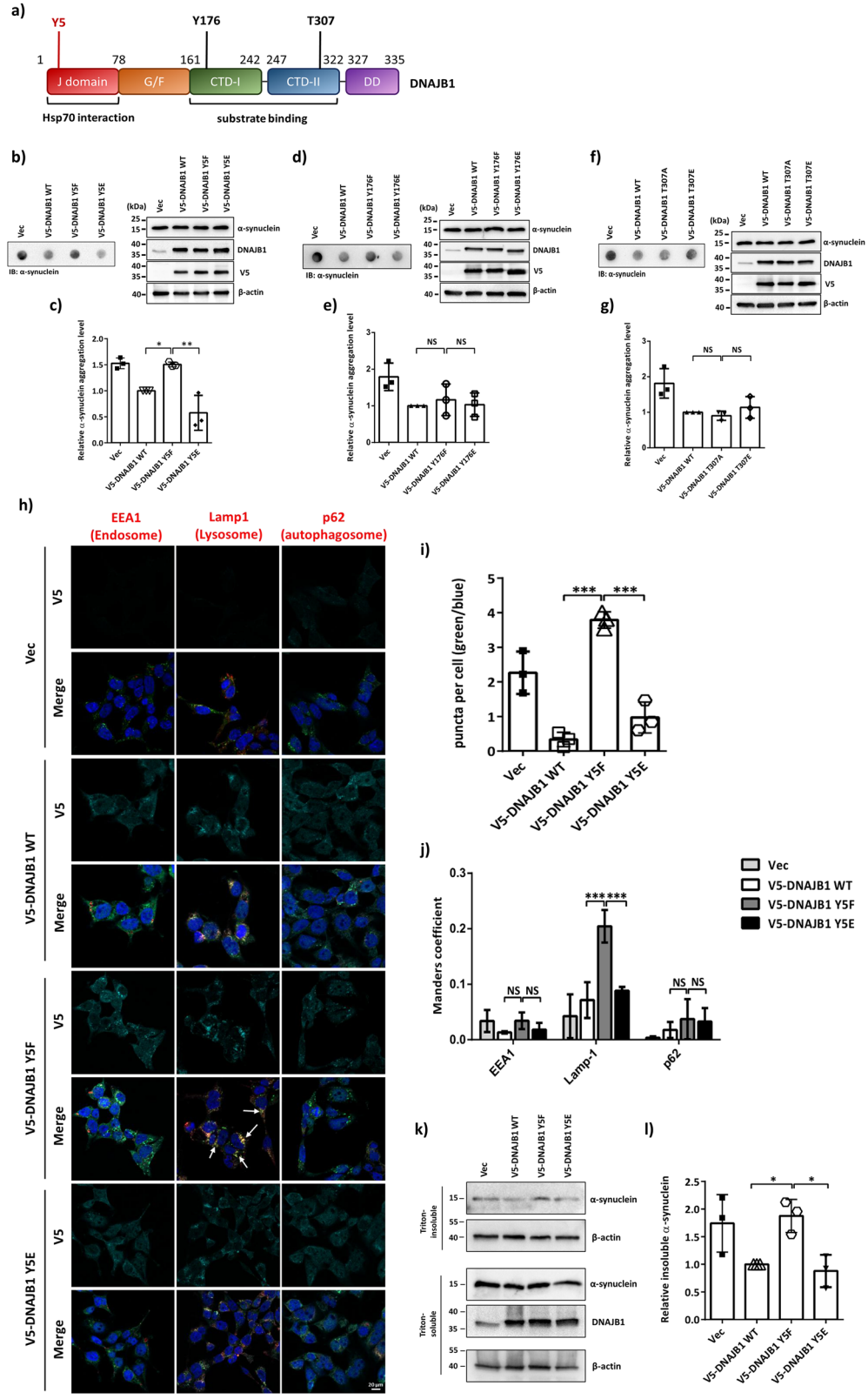

by filter trap assay. As shown in Fig. 2b–g, tyrosine 5 (Y5), but not Y176 and T307 phosphorylation, facilitates DNAJB1 to reduce α-synuclein aggregates. To further confirm the role of Y5 phosphorylation on DNAJB1 in modulating α-synuclein aggregation, we visualized the aggregates of α-synuclein in stress-induced SH-SY5Y cells by confocal microscopy. Compared to the wild-type (WT) expression cells, a greater number of aggregated puncta were observed in the Y5F mutant group (Fig. 2h, i), along with an increased colocalization between the puncta and lysosomes in the Y5F mutant group (Fig. 2h, j). Quantitative reverse transcription PCR (qRT-PCR) was used to analyze whether DNAJB1 overexpression changes in the mRNA level of *SNCA*. In Fig. S2a, overexpression of DNAJB1 WT and mutants does not alter the mRNA level of *SNCA*. To investigate whether the

Fig. 2 | DNAJB1 Tyr5 phosphorylation is critical for resolving α-synuclein aggregation. a Phosphorylation sites annotated in the PhosphoSitePlus database (https://www.phosphosite.org) are mapped onto the domain architecture of DNAJB1. **b** Chemiluminescent images of α-synuclein, DNAJB1 (WT and Y5 mutants), and β-actin. Overexpression and site-directed mutagenesis were performed to generate dephospho-mimetic (F/A) and phospho-mimetic (D/E) variants at indicated residues. SH-SY5Y cells expressing V5-tagged DNAJB1 (WT or mutants) were pretreated with 100 nM rotenone for 24 h, followed by α-synuclein aggregation analysis via filter trap assay. Data were analyzed using one-way ANOVA with Dunnett's test. **c** Quantification of α-synuclein aggregation, normalized to β-actin, in SH-SY5Y cells expressing V5-tagged DNAJB1 WT or Y5 variants. **d** Chemiluminescent images of α-synuclein, DNAJB1 (WT and Y176 mutants), and β-actin. **e** Quantification of α-synuclein aggregation, normalized to β-actin, in SH-SY5Y cells expressing V5-tagged DNAJB1 WT or Y176 variants. **f** Chemiluminescent images of α-synuclein, DNAJB1 (WT and T307 mutants), and β-actin. **g** Quantification of α-synuclein aggregation, normalized to β-actin, in SH-SY5Y cells expressing V5-tagged DNAJB1 WT or T307 variants. **h** Following 24 h pretreatment with 100 nM rotenone, SH-SY5Y cells expressing V5-tagged DNAJB1 WT, Y5F, or Y5E were fixed and stained with anti-V5 (cyan), anti-organelle (red), and anti-α-synuclein (green) antibodies. Nuclei were counterstained with DAPI (blue). Images were captured using a Zeiss LSM780 confocal fluorescence microscope. Scale bar: 20 μm. **i** The numbers of puncta in the cells were quantified from 3 fields. Data was analyzed by one-way ANOVA with Dunnett's test. **j** Colocalization analysis between α-synuclein (green) and each organelle (red) from 3 fields. Data was analyzed by two-way ANOVA with Dunnett's test. **k** SH-SY5Y cells expressing V5-tagged DNAJB1 WT, Y5F, or Y5E were harvested following 24 h rotenone treatment. Lysates were biochemically fractionated into Triton-soluble and -insoluble fractions, and DNAJB1 expression along with α-synuclein distribution was assessed by western blotting. β-actin served as a loading control. **l** Quantification of α-synuclein insoluble form in (**k**). The Triton-insoluble form of α-synuclein was normalized to β-actin. Data were analyzed by one-way ANOVA with Dunnett's test. Each dataset is expressed as mean ± SD for $n = 3$. $^{*}P < 0.05$, $^{**}P < 0.01$, $^{***}P < 0.001$.

Table 2 | Kinase was predicted and scored by the Netphos-3.1 website (https://services.healthtech.dtu.dk/services/NetPhos-3.1/)

Amino acids sequence of Dnajb1	Phosphorylation site	Kinase	Score
MGKDYYQTL	Tyr5	InsR	0.491
		EGFR	0.379
		SRC	0.311
		unsp	0.119

changed α-synuclein protein aggregation was caused by alteration of the levels of heat shock proteins and GBA, the protein levels of a subset of Hsp70s (HSPA8 and HSPA1A) were detected by western blotting in V5-tagged DNAJB1 WT and mutant DNAJB1 expressing SH-SY5Y cells. Overexpression of V5-tagged DNAJB1 WT and mutant DNAJB1 does not change the protein levels of these Hsp70 molecular chaperones and GBA (Fig. S2b–f). Overexpression of V5-tagged DNAJB1 WT and mutant DNAJB1 does not cause EGFR and GBA to colocalize with endosomes, lysosomes, or autophagosomes (Fig. S2g–j). Additionally, cell fractionation analysis showed that the level of insoluble α-synuclein in the Y5F mutant group was higher than in the WT and Y5E groups (Fig. 2k, l). These data indicate that the Y5F mutation loses DNAJB1's ability to clean up α-synuclein aggregation. Together, these results suggest that Y5 phosphorylation is a key signal for boosting DNAJB1's activity.

EGFR regulates Tyr5 phosphorylation on DNAJB1

To investigate which kinase is responsible for Y5 phosphorylation of DNAJB1, we generated phosphor-specific antibodies (Fig. S3). Netphos-3.1 kinase prediction program was used to predict the potential kinase of DNAJB1 Y5 phosphorylation, and the insulin receptor (INSR) and EGFR rank at the top two kinases of the prediction (Table 2). The ratio of phosphorylated AKT and EGFR served as the indicator of these two kinase inhibitors, respectively. We compared the phosphorylation status of DNAJB1 Y5 in SH-SY5Y cells treated with the INSR inhibitor NVP-AEW541 or the EGFR inhibitor afatinib. Notably, the EGFR inhibitor afatinib, but not the INSR inhibitor NVP-AEW541, specifically inhibited the Y5 phosphorylation (Fig. 3b, e). The drug efficacy was confirmed by immunoblotting (Fig. 3c, f). The results determine the specificity of EGFR on DNAJB1 Y5 phosphorylation. To examine whether afatinib treatment alters the localization of EGFR, confocal microscopy analysis was conducted. In Fig. 3g, h, afatinib treatment inhibits the colocalization between EGFR and lysosome. Given that the EGFR-lysosomal degradation pathway is initiated when EGFR activates[34], these results further verify the effectiveness of afatinib (Fig. 3g, h).

Y5 of DNAJB1 is a direct target of phosphorylation by EGFR

To confirm whether EGFR is the kinase for Y5 phosphorylation of DNAJB1, we used lentivirus to knock down EGFR in SH-SY5Y cells. Compared to the knockdown of firefly luciferase (shLuc) control cells, the knockdown of EGFR resulted in the lower phosphorylation status of DNAJB1 Y5 (Fig. 4a, b). The knockdown efficiency was analyzed at the protein level by immunoblotting (Fig. 4c). Therefore, the knockdown of EGFR blocks DNAJB1 Y5 phosphorylation.

To further examine whether DNAJB1 Y5 is a direct EGFR substrate, an in vitro kinase assay was conducted. *Escherichia coli* (*E. coli*) expressed and purified full-length DNAJB1 was used as a substrate for phosphorylation by commercially active EGFR. The phosphorylated protein was detected by phosphor-specific antibodies. As the data shown in Fig. 4d, e, active EGFR phosphorylates purified DNAJB1, and Y5F mutant failed to be phosphorylated, indicating that Y5 is a direct target of EGFR.

Downregulated EGFR impairs the ability of DNAJB1 to resolve α-synuclein aggregation

To explore the association between EGFR phosphorylation at Y5 of DNAJB1 and DNAJB1-mediated resolution of α-synuclein aggregation, lentiviral-mediated EGFR knockdown was employed in SH-SY5Y cells. Compared to the shLuc control group, EGFR knockdown resulted in elevated levels of α-synuclein aggregation (Fig. 5a, b). Furthermore, despite DNAJB1 overexpression in these cells, increased α-synuclein aggregation persisted under conditions of EGFR knockdown (Fig. 5c, d), demonstrating that DNAJB1-mediated clearance of α-synuclein aggregation relies on EGFR.

DNAJB1 Y5 phosphorylation promotes the DNAJB1-HSC70/HSP70 interaction

Structural analysis using AlphaFold revealed that the DNAJB1 protein contains one J domain, one G/F-rich region, two C-terminal domains (CTD), and one dimerization domain (DD) (Fig. 6a, b). Y5 is located within the Hsp70 interaction domain and particularly in the first alpha helix of DNAJB1 (Fig. 6a, b). According to the DynaMut prediction of Y5 mutants, the stability of DNAJB1 Y5E significantly decreased while the flexibility of the first alpha helix increased (Fig. S5a). The interaction of all members in the JDP family with Hsp70 is mediated through their conserved J-domain that binds to Hsp70 and triggers ATP hydrolysis[35,36]. These prompted us to evaluate whether DNAJB1 Y5 phosphorylation affects the Hsp70 folding system in neuronal cells. Given that HSPA8/HSC70 is constitutively expressed and HSPA1A/HSP70 can be induced by stress in the cytoplasm[37], we treated rotenone as a stressor to investigate the interaction between these two chaperones and DNAJB1. To determine the interactions between DNAJB1 mutants and HSPA8, we performed a proximity ligation assay

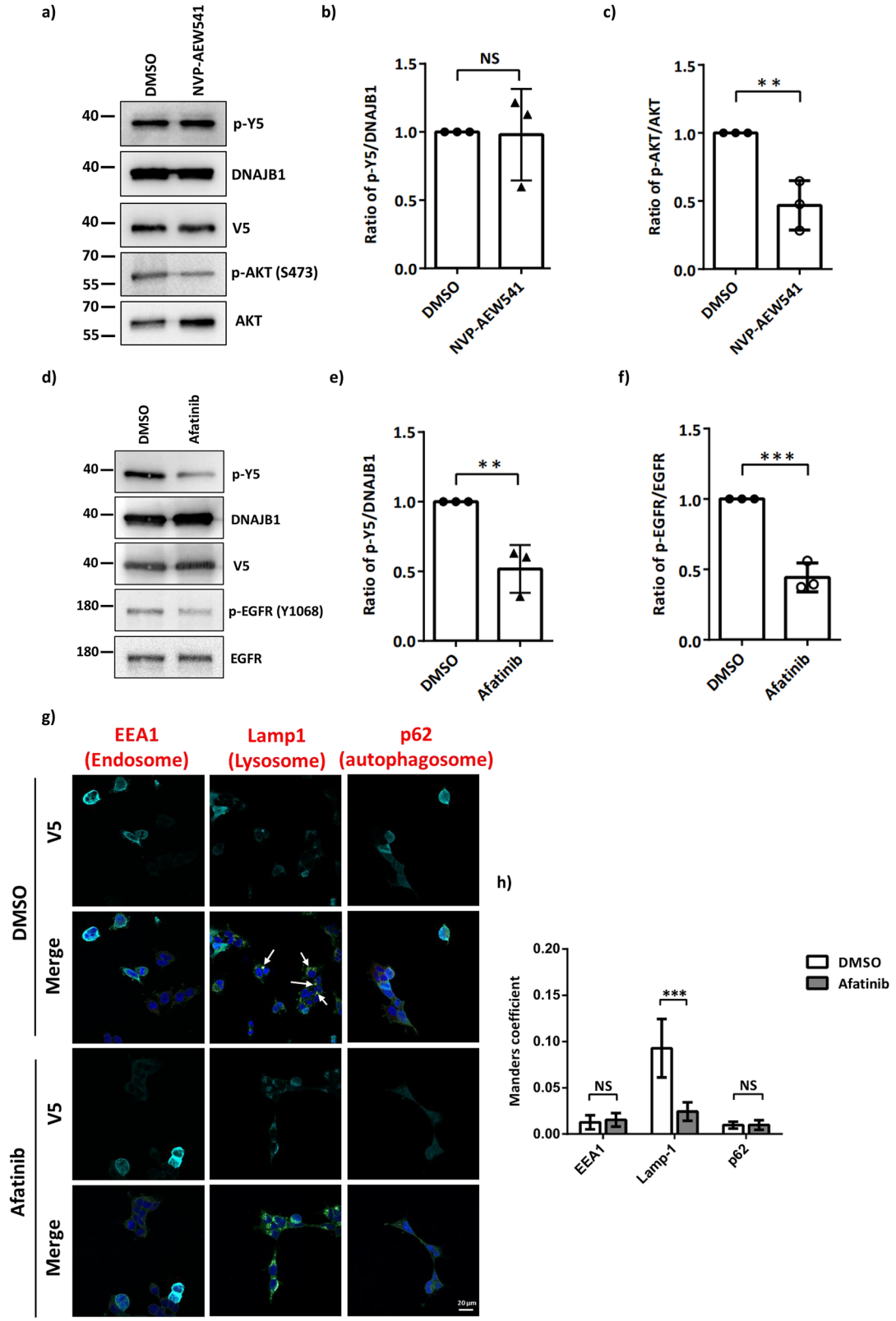

Fig. 3 | EGFR regulates DNAJB1 Y5 phosphorylation. a Chemiluminescent images of p-Y5, DNAJB1, p-AKT(Ser473) and AKT. Detection of DNAJB1 phosphorylation and determination of the potential kinase by the homemade anti-phosphor-Y5 antibodies. After 24 h transfection with V5-DNAJB1, SH-SY5Y cells were treated with indicated INSR inhibitor (NVP-AEW541) for 2 h. DNAJB1 phosphorylation was detected by the anti-phosphor-Y5-specific antibody. Data was analyzed by unpaired two-tailed Student's t-test. **b** The ratio of p-Y5/ DNAJB1 after NVP-AEW541 treatment. **c** The effectiveness of NVP-AEW541 was confirmed by the phosphorylation of AKT. **d** Chemiluminescent images of p-Y5, DNAJB1, p-EGFR(Tyr1068) and EGFR. **e** The ratio of p-Y5/ DNAJB1 after EGFR inhibitor (afatinib) treatment. **f** The effectiveness of afatinib was confirmed by the phosphorylation of EGFR. **g** After 2 h treatment with 2.5 μM afatinib, V5-tagged DNAJB1 WT expressing SH-SY5Y cells were fixed and stained with anti-V5 (cyan), anti-organelle (red), and anti-EGFR (green) antibodies. Nuclei were counterstained with DAPI (blue). Images were captured using a Zeiss LSM780 confocal fluorescence microscope. Scale bar: 20 μm. **h** Colocalization analysis between EGFR (green) and each organelle (red) from 3 fields. Data were analyzed by two-way ANOVA with Sidak's test. Each dataset is expressed as mean ± SD for $n = 3$. $^{**}P < 0.01$, $^{***}P < 0.001$.

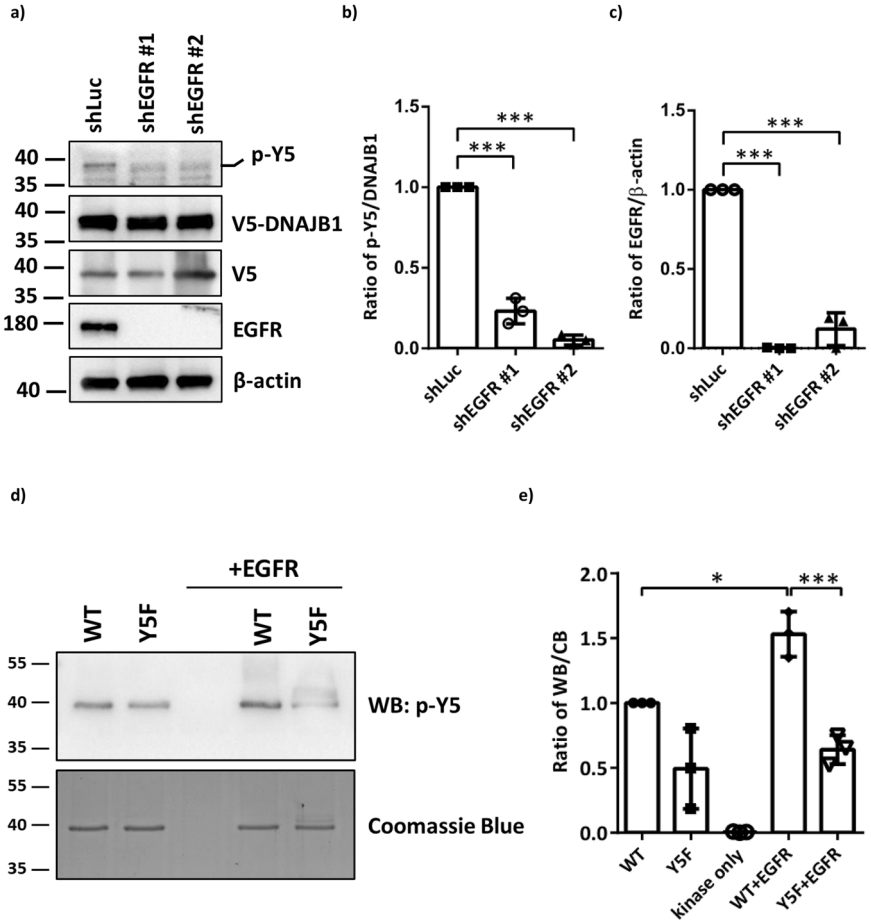

Fig. 4 | EGFR directly phosphorylates DNAJB1 at Y5. a Chemiluminescent images of p-Y5, DNAJB1, EGFR and β-actin. shLuc or shEGFR SH-SY5Y cells were transfected with 1 μg V5-DNAJB1 WT for 24 h. DNAJB1 Y5 phosphorylation and knockdown of EGFR were determined by western blotting using Y5 phosphor-specific antibodies and EGFR antibodies, respectively. β-actin was used as a loading control for normalization. **b** Quantification of Y5 phosphorylation in shEGFR SH-SY5Y cells. **c** The knockdown efficiency of EGFR. **d** EGFR phosphorylates DNAJB1 Y5 in vitro. In vitro EGFR kinase assay was conducted using commercially active EGFR on *E. coli* purified recombinant His6-DNAJB1 and His6-DNAJB1 Y5F substrates. Samples were loaded onto a 10% SDS-PAGE, and the phosphorylated proteins were detected by phosphor-specific antibodies (upper panel). The same samples were stained with Coomassie blue to confirm that all proteins were equally loaded (bottom panel). **e** The ratio of p-Y5/ total protein. Data were analyzed by one-way ANOVA with Dunnett's test. Each dataset is expressed as mean ± SD for $n = 3$. $^{*}P < 0.05$, $^{***}P < 0.001$.

(PLA) under the overexpression of Myc-tagged α-synuclein A53T in SH-SY5Y cells. The confocal images showed that the ratio of positive foci in the DNAJB1 Y5F group is less than that in the WT or Y5E group (Fig. 6c, d), indicating that the association between DNAJB1 and HSPA8 would be enhanced under DNAJB1 Y5 phosphorylation. Since the Y5 residue is in the J-domain of DNAJB1, phosphorylation of Y5 may alter the structure of the J-domain and result in a higher binding affinity to the HSPA8 chaperone (Fig. S3b).

To further examine whether DNAJB1 Y5 phosphorylation controls the interaction with HSC70/HSP70, we conducted a co-immunoprecipitation (co-IP) assay. The co-IP results indicated that DNAJB1 exhibited interaction with HSPA8 and HSPA1A (Fig. 6e). The co-IP efficiency of DNAJB1 Y5F mutant was relatively lower than that of DNAJB1 WT and Y5E mutant, suggesting that DNAJB1 Y5 phosphorylation increases the binding ability between DNAJB1 and the cytoplasmic Hsp70 families (Fig. 6f, g). Together with the PLA and co-IP results, we conclude that the Y5 phosphorylation may promote the interaction between DNAJB1 and HSC70/HSP70.

The expression levels of EGFR and DNAJB1 are reduced, but phosphorylation of DNAJB1 is increased, in the brain tissue of individuals with PD

Based on the findings presented in Fig. 7, it is evident that EGFR plays a crucial role in facilitating DNAJB1-mediated resolution of α-synuclein aggregation. To further explore the relationship between DNAJB1 and the progression of PD, we detected the expression levels of EGFR, DNAJB1, and phosphorylated EGFR and DNAJB1 Y5 using human brain lysates obtained from three pairs of neurologically normal individuals and PD patients. Notably, a decrease in the levels of not only DNAJB1 but also EGFR in the brain lysates of the PD patients compared to the unaffected controls was observed (Fig. 8a–c). And, not only the phosphorylation status of DNAJB1 Y5 but also the ratio of phosphorylated EGFR in PD patients was higher than that in the unaffected controls (Fig. 8a, d, e). Furthermore, the results of the DNAJB1 co-IP assay showed an increased interaction between EGFR and DNAJB1 in the brain lysates derived from PD patients compared to that of the controls (Fig. 8e, f). These observations indicate a diminished EGFR-DNAJB1 expression along with a capability of EGFR-dependent DNAJB1 activation in resolving aggregated α-synuclein in individuals with PD.

Discussion

In this study, we discovered a DNAJB1-dependent clearance of α-synuclein in neuronal cells, and the phosphorylation on DNAJB1 tyrosine 5 plays a critical role in this process. Moreover, our data indicates that EGFR phosphorylates DNAJB1 tyrosine 5 directly. It coordinates the subsequent recruitment of the client α-synuclein to the Hsp70 folding system, ensuring proper folding of α-synuclein and preventing pathogenic α-synuclein aggregations in the PD progress.

PD is characterized by a progressive degeneration of neurological function. Its etiology is deemed multifaceted, posited to result from a complex interplay between aging, genetic predispositions, and environmental influences. Nonetheless, the full complexity of its origins remains yet to be fully elucidated. Numerous gene mutations, including *SNCA*, *LRRK2*, *PRKN*, *DJ1*, *PINK1*, and *ATP13A2*, have been identified to link to familial parkinsonism[38]. However, these mutations account for less than ten percent of patients with PD[39]. Aside from genetic factors, evidence has shown that environmental factors may play a major contributor, including traumatic brain injury, heavy metals exposure, air pollution, pesticides, and herbicides, which all can be sources of environmental stress[40]. According to our findings, there may exist a robust correlation between the expression level of DNAJB1 and the clearance of α-synuclein in neurons. The expression level

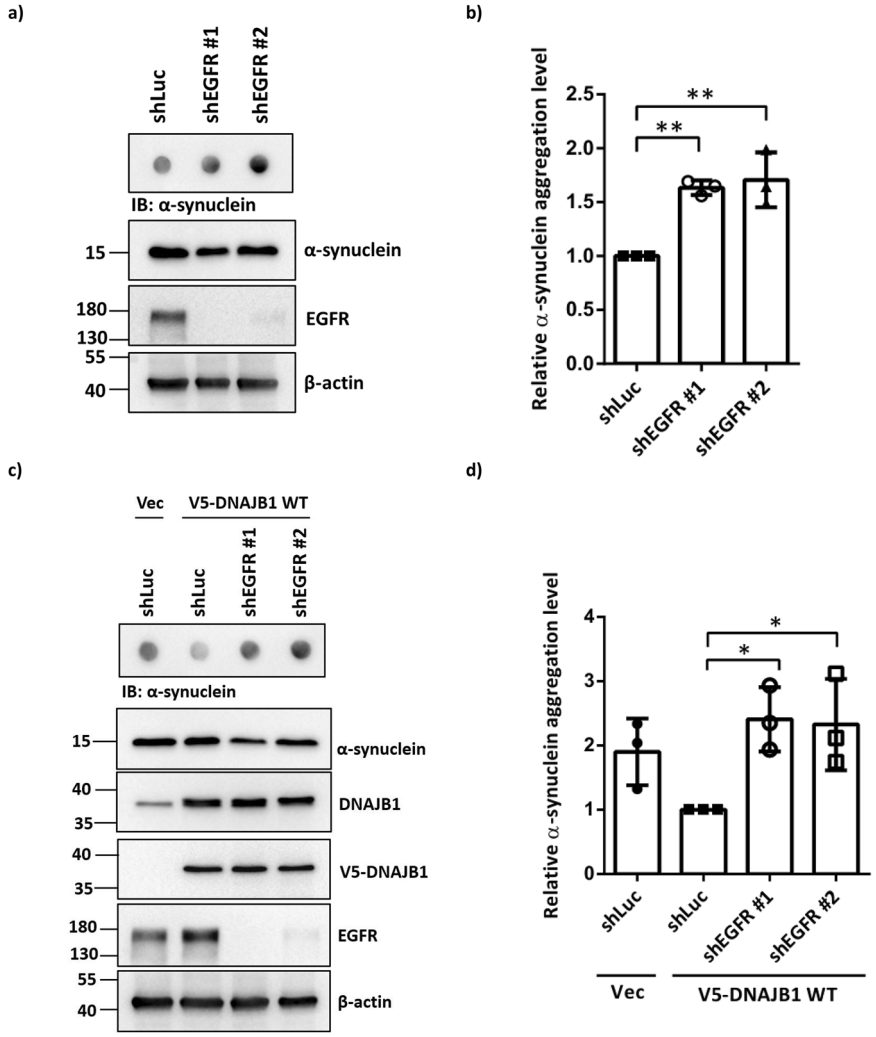

Fig. 5 | Knockdown of EGFR induces α-synuclein aggregation. a After 24 h rotenone treatment, shEGFR SH-SY5Y cells were harvested. The filter trap assay was employed to detect α-synuclein aggregation. The α-synuclein expression and EGFR knockdown were confirmed by western blotting. **b** Quantification of α-synuclein aggregation levels, normalized with β-actin, in (**a**). **c** After 24 h rotenone treatment, shEGFR SH-SY5Y cells were transfected with 1 μg V5-tagged DNAJB1 WT for 48 h and followed by analysis of α-synuclein aggregation via filter trap assay. The α-synuclein expression, DNAJB1 overexpression, and EGFR knockdown were confirmed by western blotting. **d** Quantification of α-synuclein aggregation levels, normalized with β-actin, in (**c**). Data were analyzed by one-way ANOVA with Dunnett's test. Each dataset is expressed as mean ± SD for $n = 3$. $^{*}P < 0.05$, $^{**}P < 0.01$.

of DNAJB1 is comparatively diminished in the brains of PD patients. Consequently, a reduction in DNAJB1 may lead to further accumulation of α-synuclein aggregates in the PD brains. This phenomenon may constitute one of the contributory factors to the pathogenesis of PD.

In addition to external environmental stressors, alterations in internal signal transduction pathways may lead to epigenetic and posttranslational alterations that may exert a substantial influence on disease development. Amino acid modifications can profoundly impact protein-protein interactions, particularly when localized at binding interfaces or active site crevices. These alterations possess the capacity to impede access to the active site, modify recognition motifs, alter specificity, or modulate binding affinity. In this study, Y5 phosphorylation on DNAJB1 is critical for regulating its activity and can promote its interaction with Hsp70. This phosphorylation may play a crucial backup role in reducing inappropriate protein aggregation, suggesting a potential link between DNAJB1 phosphorylation dynamics and the pathogenesis of PD.

EGFR is a receptor for growth factors that induce cell differentiation and proliferation. EGFR is a receptor tyrosine kinase that, when activated by its ligands, undergoes autophosphorylation on specific tyrosine residues. This activation triggers downstream signaling pathways that can influence cell survival, proliferation, and stress responses. Numerous investigations have concentrated on elucidating the expression levels of EGFR in individuals afflicted with PD. A clinical study has demonstrated a reduction in plasma EGF levels among PD patients compared to unaffected controls[22]. In addition, clinical analyses have revealed a notable correlation between EGFR polymorphisms and the susceptibility to PD evidenced in biological specimens[24]. Consequently, it is conceivable that forthcoming therapeutic strategies for PD may prioritize the maintenance of EGFR activity and the augmentation of EGFR expression levels, given the robust association observed between EGFR and PD pathogenesis. Moreover, a decreased EGFR expression level is observed in DNAJB1 knockdown A549 cells[41]. All these observations suggest a regulation between EGFR and DNAJB1 is bidirectional.

Based on the predicted structure of DNAJB1 (Fig. 6a, b and S5), we hypothesize that the DNAJB1 Y5F mutant exhibits increased hydrophobicity within the J-domain, potentially reducing the interaction between the J-domain and Hsp70. This hypothesis is supported by PLA and co-IP analyses. However, the exact structure of DNAJB1 remains unknown, limiting further exploration of downstream signaling pathways and molecular mechanisms. Obtaining the actual DNAJB1 structure in the future would provide a more comprehensive understanding of the underlying mechanisms.

Lung cancer and PD were considered unrelated conditions in the past. However, recent emerging evidence indicates that they may share common risk factors such as aging, and also exhibit some overlapping genetic features[42]. A previous study reported a lower-than-expected incidence of lung cancer among patients with PD[43], and many subsequent studies confirmed this finding[44,45]. It indicates the overlapping function of the PD gene family between two diseases. Specifically, certain genes implicated in PD have also been implicated in the pathology of lung cancer. For instance, the depletion of *LRRK2*, a key gene associated with PD, enhances the development of lung tumors[46].

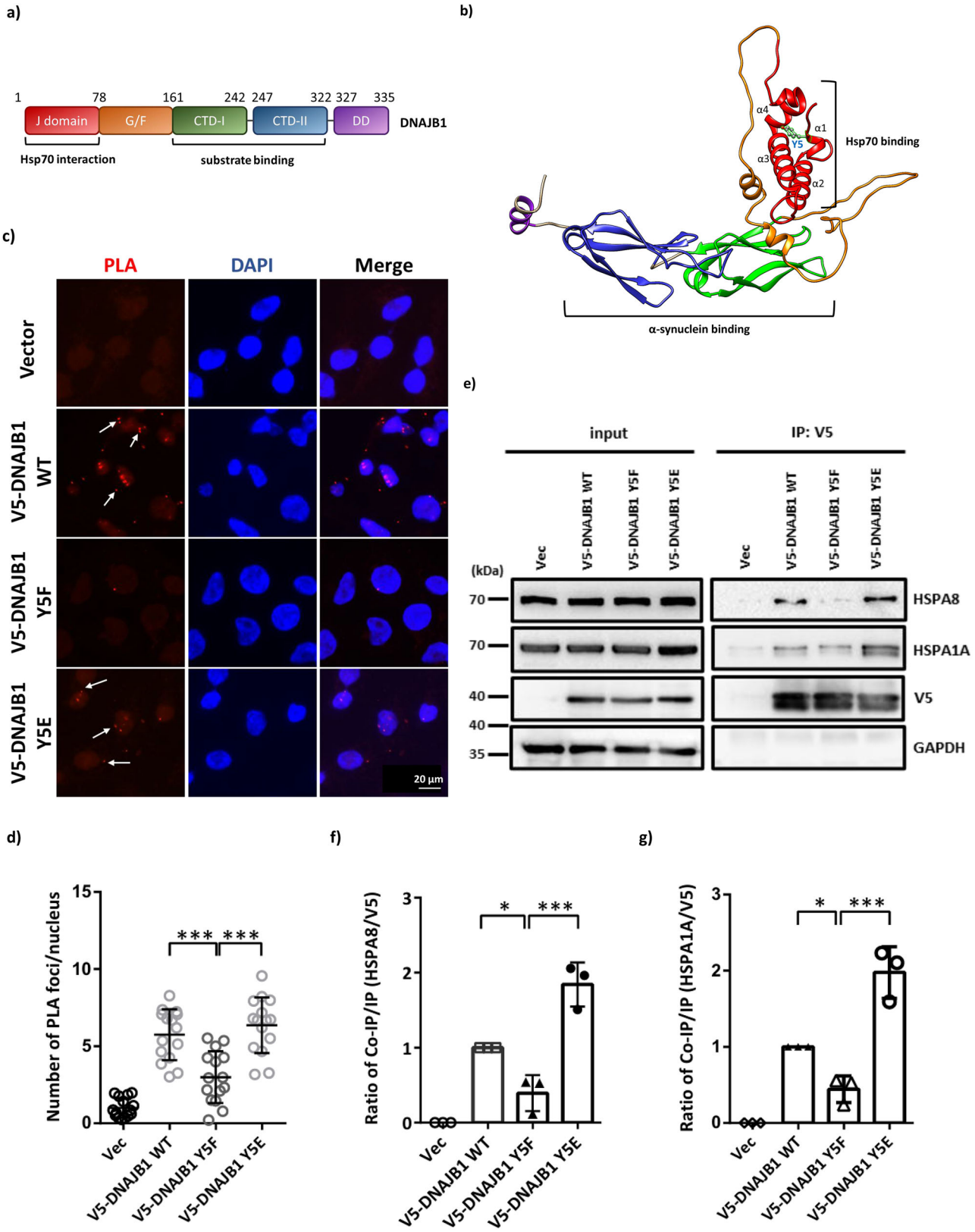

SNCA is downregulated and functions as a tumor suppressor in lung adenocarcinoma according to bioinformatic analysis[47]. Given that overexpressed *SNCA* induces mitochondria-mediated apoptosis leading to neuronal death, it is reasonable to believe the decreased risk of lung cancer observed in PD may be linked to increased apoptosis in cancer cells. Furthermore, as mentioned above, the augmentation of EGFR expression levels is a potential strategy for PD therapy. From our perspective, if patients diagnosed with both PD and lung cancer are treated with this therapeutic strategy, it is advisable to monitor the progression of the tumor closely. In our study, a notable decrease in the

Fig. 6 | The interaction between DNAJB1 and Hsp70 families. a The primary structure of DNAJB1. **b** The structure of DNAJB1 was predicted by Alphafold 2 with Y5 labeled in light blue. **c** SH-SY5Y cells transiently expressed V5-tagged WT or mutant DNAJB1 along with Myc-tagged α-synuclein A53T. After 24 h post-transfection, cells were seeded on slides for an additional 24 h. Cells seeded on slides were then hybridized with V5 and HSPA8 primary antibodies to detect the interaction between DNAJB1 (WT and mutant) and HSPA8. When DNAJB1 and HSPA8 interacted, the PLA probes on secondary antibodies were ligated and amplified. The red PLA signals showing protein interaction were detected by a Zeiss LSM780 confocal fluorescence microscope. Scale bar: 20 μm. **d** Quantification of PLA assay in (**c**). **e** After 24 h rotenone pretreatment, V5-tagged DNAJB1 WT or mutant DNAJB1 expressing SH-SY5Y cell lysates were precipitated by V5 antibodies, and the products were detected for the co-purification of the endogenous Hsp70 (HSPA8 and HSPA1A). The bands below V5 and HSPA1A are truncated protein species. **f** Comparison of the interaction between DNAJB1 and HSPA8 in V5-tagged DNAJB1 WT or mutant DNAJB1 groups. **g** Comparison of the interaction between DNAJB1 and HSPA1A in V5-tagged DNAJB1 WT or mutant DNAJB1 groups. Data were analyzed by one-way ANOVA with Dunnett's test. Each dataset is expressed as mean ± SD for $n = 3$. $^{*}P < 0.05$, $^{***}P < 0.001$.

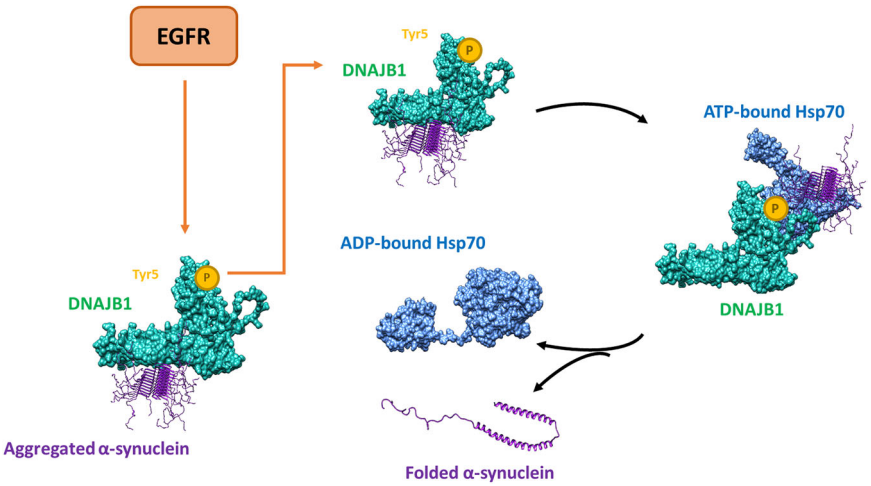

Fig. 7 | DNAJB1 facilitates the delivery of aggregated α-synuclein to the Hsp70 chaperone machinery within neuronal cells. ATP hydrolysis induces a conformational change in Hsp70, resulting in the closure of its substrate-binding domain. Subsequently, a nucleotide exchange factor catalyzes the replacement of ADP with ATP, promoting the release of properly folded α-synuclein. Phosphorylation of DNAJB1 at tyrosine residue 5 enhances its capacity to disaggregate α-synuclein, a process that is contingent upon prior phosphorylation of DNAJB1 mediated by EGFR.

expression levels of EGFR and DNAJB1 is observed in the postmortem brain lysates of PD patients compared to the unaffected controls. Additionally, there is a significant increase in the ratios of phosphorylated Y5 of DNAJB1 and phosphorylated EGFR in the brains of PD patients, suggesting a compensatory mechanism of DNAJB1 phosphorylation in PD patients. These data strongly imply that EGFR-dependent phosphorylation of DNAJB1 at Y5 plays an important role in the folding of α-synuclein in PD.

In conclusion, we have found that the clearance of α-synuclein in neuronal cells relies on DNAJB1, with phosphorylation at tyrosine 5 of DNAJB1 playing a crucial role in this process. Additionally, our data suggests that EGFR directly phosphorylates DNAJB1 at this site. These results not only provide insights into the mechanisms underlying PD pathology but also position DNAJB1 as a potential therapeutic target. Based on our study, DNAJB1 can resolve α-synuclein aggregates and is modulated by EGFR; theoretically, EGFR activators could enhance DNAJB1 phosphorylation at tyrosine 5, potentially slowing down PD progression. However, given that EGFR is an oncogene, this approach carries an increased risk of cancer. Thus, further challenges must be resolved before this strategy can be translated into clinical use.

Methods

Cell culture and reagents

HEK-293T cells were maintained in Dulbecco's modified Eagle's medium (DMEM) high glucose (Cytiva, Logan, UT, USA) supplied with 10% fetal bovine serum (FBS), 1x penicillin/streptomycin/fungizone. SH-SY5Y cells were obtained from ATCC and cultured in DMEM/F12 (44.5/44.5%) medium (Cytiva) supplied with 10% FBS and 1x penicillin/streptomycin/fungizone. All cell lines were cultured under standard conditions (37 °C, 5% CO_2) and routinely tested for the absence of mycoplasma. To induce the aggregation of α-synuclein in SH-SY5Y cells, cells were treated with 100 nM rotenone (Sigma-Aldrich, Louis, MO, USA) for 24 h before analysis. The lysates of this pretreatment were conducted in filter trap assay, immunostaining, cell fractionation analysis, and co-IP analysis.

The InsR inhibitor, NVP-AEW541 (MedChem Express, Princeton, NJ), and the EGFR inhibitor, afatinib (MedChem Express, Princeton, NJ) were utilized in the cell toxicity assay. A range of afatinib concentrations (0.625, 1.25, 2.5, 5, and 10 μM) was applied to evaluate cellular viability. It was observed that afatinib concentrations exceeding 2.5 μM induce cell death. Similarly, various concentrations of NVP-AEW541 (0, 1, 2, 5, 10, and 50 μM) were tested to assess the cellular response, with concentrations above 10 μM leading to cell mortality. Finally, inhibitor treatments were administered for 2 h at concentrations of 2.5 μM (afatinib) and 10 μM (NVP-AEW541), respectively.

Transfection

After seeding 2×10^5 SH-SY5Y cells in a 6-well plate for 24 h, 2 μg plasmids were transfected using Lipofectamine LTX with Plus Reagent (DNA: Plus: LTX = 1:1:2) (Thermo Fisher Scientific, Waltham, MA, USA) and 500 μl OPTI-MEM. DNA: Plus reagents were mixed well in OPTI-MEM. Then, the solution was stored at room temperature for 15 min and spun down, followed by adding LTX reagent. Before adding it to the culture plate, the solution was mixed well and spun down, stored at room temperature for 30 min.

Lentivirus production and infection

HEK-293T cells were co-transfected with the packaging plasmid (pCMV-Δ8.91), envelope (pMD.G), and either hairpin pLKO-RNAi vectors for the virus production. The specific oligonucleotide sequences of shRNA are listed in Table S1. After 24 h post-transfection, the medium was replaced by DMEM containing filtered 1% BSA medium. Virus-containing supernatants were collected after 48 h and 72 h post-transfection. For a 6-well culture, 1 × 105 SH-SY5Y cells were infected with each virus plus DMEM/F12 medium containing 0.8 μg/ml

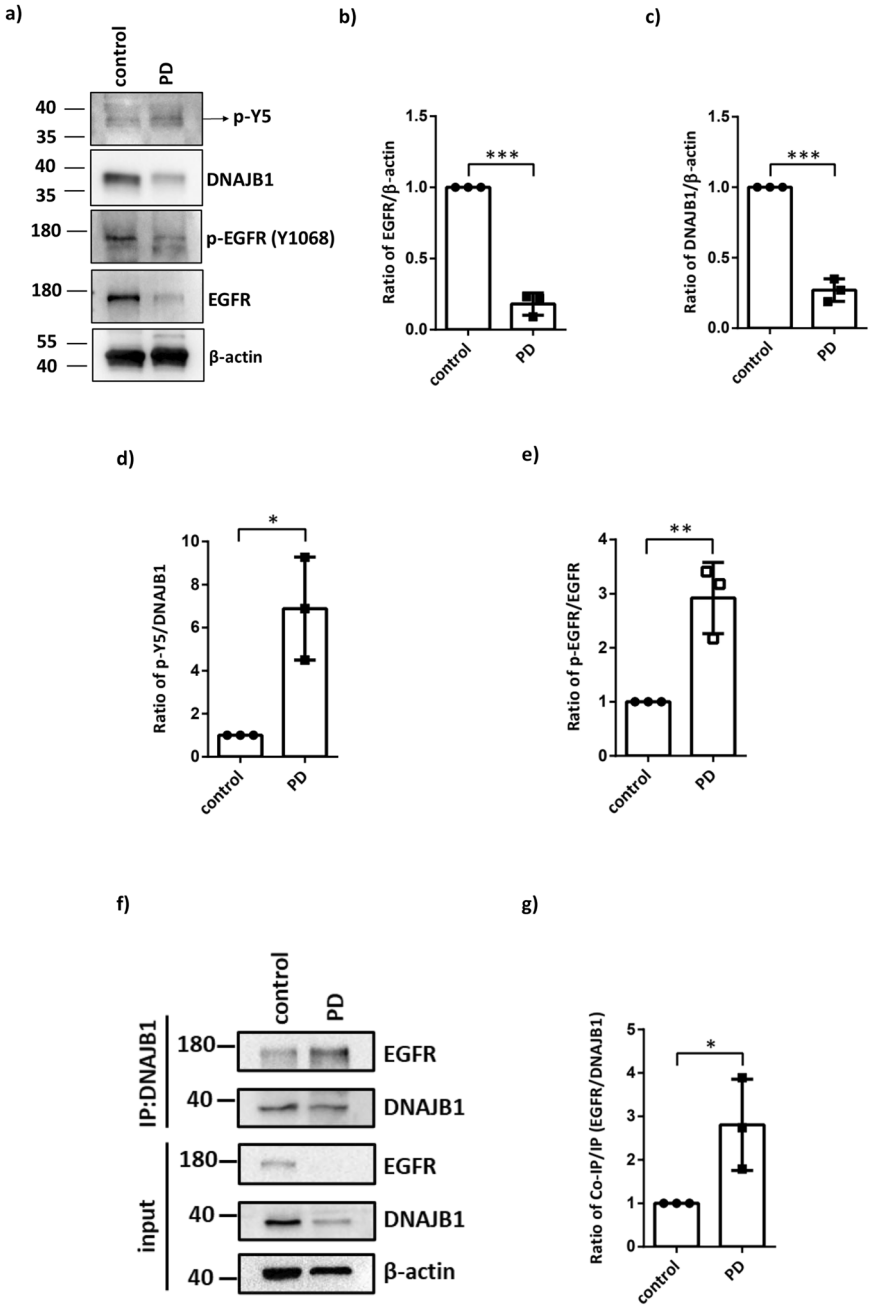

Fig. 8 | The comparison of EGFR, DNAJB1, and phosphorylated DNAJB1 Tyr5 and EGFR between human controls and PD patients.
a Chemiluminescent images of p-Y5, DNAJB1, p-EGFR (Tyr1068), EGFR and β-actin. Protein expression levels of brain lysates from three different pairs of human controls and PD patients. **b** Quantification of EGFR amounts in (**a**). **c** Quantification of DNAJB1 amounts in (**a**). **d** Quantification of phosphorylated DNAJB1 Y5 amounts in (**a**). **e** Quantification of phosphorylated EGFR amounts in (**a**). **f** DNAJB1 IP products were detected for the co-purification of the endogenous EGFR. **g** Comparison of the interaction between DNAJB1 and EGFR. The data in (**f**, **g**) is three independent experiments in one patient. All data were analyzed by unpaired two-tailed Student's t-test. Each dataset is expressed as mean ± SD for $n = 3$. $^{*}P < 0.05$, $^{**}P < 0.01$, $^{***}P < 0.001$.

polybrene (Millipore, Billerica, MA, USA) for 24 h. The transduced cells were selected with DMEM/F12 medium containing 1 μg/ml puromycin (Sigma-Aldrich) for the indicated days.

Analysis of brain tissue

Brain tissue was lysed with an immunoprecipitation buffer (1% Triton X-100, 150 mM NaCl, 10 mM NaH_2PO_4, 15 mM Na_2HPO_4, 50 mM NaF, 1 mM Na_3VO_4) on ice for 5 min. Subsequently, the sample was boiled in 5x SDS sample buffer. The sample was then analyzed using western blotting. All used brain tissues and antibodies are listed in Table 3.

Plasmids

The pcDNA5/FRT/TO/V5 vector was acquired from Addgene #19445 and the pcDNA5/FRT/TO/V5 DNAJB1 was purchased from Addgene #19522. Then, the pcDNA5/FRT/TO-V5-DNAJB1 Y5F, pcDNA5/FRT/TO-V5-DNAJB1 Y5E, pcDNA5/FRT/TO-V5-DNAJB1 Y176F, pcDNA5/FRT/TO-V5-DNAJB1 Y176E, pcDNA5/FRT/TO-V5-DNAJB1 T307A, and pcDNA5/FRT/TO-V5-DNAJB1 T307E were generated by site-directed mutagenesis[10,26].

Next, these plasmids were constructed by the T4 ligation method. As for the J domain proteins, the pcDNA5/FRT/TO-V5-DNAJB1 WT and Y5F were both digested with BamHI-HF and NotI-HF as "insert" and ligated to restriction enzyme digested pET-28a vector with T4 ligase. All plasmid sequences are listed in Table S1.

Generation of phospho-DNAJB1 (Tyr5) antibody

To generate the phospho-DNAJB1 (Tyr5) polyclonal antibody, synthetic phosphopeptide (M-G-K-D-pY-Y-Q-T-L-G-L-A-R-G-A-C) was purchased from Kelowna International Scientific Inc. (New Taipei City, Taiwan). A 2 mg peptide containing a terminal cysteine was conjugated to Keyhole Limpet Hemocyanin (KLH) proteins utilizing the ImjectTM Maleimide-Activated mcKLH Spin Kit following the protocols prescribed by the manufacturer (Thermo Scientific). 50 μl of the peptide-KLH conjugates were administered intraperitoneally into a naive Balb/c mouse.

Table 3 | List of key resources

REAGENT or RESOURCE	SOURCE	IDENTIFIER
Antibodies		
α-synuclein (1:1000 dilution for Western blot) (1:250 dilution for IF)	GeneTex	112799, RRID: AB_10618470
DNAJB1 (1:1000 dilution)	Enzo Life Science	ADI-SPA-400-D, RRID: AB_2039237
DNAJB2 (1:500 dilution)	GeneTex	104464, RRID: AB_1950126
DNAJB6 (1:2000 dilution)	Abcam	198995, RRID: AB_2924896
GAPDH (1:1000 dilution)	GeneTex	100118, RRID: AB_1080976
β-actin (1:2000 dilution)	Proteintech	60008-1-Ig, RRID: AB_2289225
HSPA8 (1:1000 dilution)	Novus	120-2788, RRID: AB_2120309
V5 (1:2000 dilution for Western blot) (1:250 dilution for IF)	Thermo Fisher Scientific	R960-25, RRID: AB_2556564
V5 (1:100 dilution for IF)	GeneTex	29137, RRID: AB_370778
GBA (1:200 dilution for IF)	GeneTex	101267, RRID: AB_10724323
HSPA1A (1:1000 dilution)	Santa Cruz	66048, RRID: AB_832518
p-EGFR(Y1068) (1:500 dilution)	Cell Signaling Technology	3777, RRID: AB_2096270
EGFR (1:1000 dilution for Western blot) (1:100 dilution for IF)	Cell Signaling Technology	4267, RRID: AB_2895042
p-AKT(S473) (1:1000 dilution)	Cell Signaling Technology	9271, RRID: AB_329825
AKT (1:1000 dilution)	Cell Signaling Technology	9272, RRID: AB_329827
EEA1 (1:200 dilution for IF)	GeneTex	634169, RRID: AB_2888419
CD107a (LAMP-1) (1:200 dilution for IF)	Invitrogen	14-1079-80, RRID: AB_467426
SQSTM1/P62 (1:200 dilution for IF)	GeneTex	629890, RRID: AB_2885144
p-Y5 (1:250 dilution for WB) (1:500 dilution for In vitro kinase assay)	This study	N/A
AlexaFluor^{R} 594 Goat Anti-mouse IgG (H + L) (1:200 dilution)	Invitrogen	A11005
Alexa Fluor™ 647 Goat anti-Rabbit IgG (H + L) (1:200 dilution)	Invitrogen	A21245
Cy^{TM}5-conjugated AffiniPure Goat Anti-Rabbit IgG (H + L) (1:200 dilution)	Jackson ImmunoResearch	111-175-144
AlexaFluor^{R} 488 Chicken Anti-goat IgG (H + L) (1:200 dilution)	Invitrogen	A21467
Biological sample		
Human brain whole tissue lysate- adult whole normal	Novus	820-59177, Lot# C511134
Human brain whole tissue lysate- adult whole PD's human	Novus	820-59407, Lot# C103261
Human brain whole tissue lysate- normal	GeneTex	28771, Lot# 822400674
Human brain whole tissue lysate- PD	GeneTex	26602, Lot# 822400902
Human brain whole tissue lysate- adult whole normal	Novus	820-59177, Lot# C807591
Human brain whole tissue lysate- adult whole PD's human	Novus	820-59407, Lot# C308158
Chemicals, peptides, and recombinant proteins		
DMEM	Cytiva	SH30022.02
DMEM/F12	Cytiva	SH30023.02
Rotenone	Sigma-Aldrich	R8875
Polybrene	Millipore	TR-1003
Protein G Mag Sepharose Xtra magnetic beads	Cytiva	28967070
Luminata^{TM} Crescendo Western HRP Substrate	Millipore	WBLUR0500
DAPI	Thermo Fisher Scientifics	D1306
Fluoromount^{TM} Aqueous Mounting Medium	Sigma-Aldrich	F4680
T-Pro non-liposome transfection reagent II	T-Pro Biotechnology	JT97-N002M
Lipofectamine^{TM} LTX reagent with PLUS^{TM} reagent	Thermo Fisher Scientific	15338100
Duolink® In Situ Wash Buffers, Fluorescence	Merck	DUO82049
Duolink® In Situ PLA® Probe Anti-Mouse PLUS	Merck	DUO92001
Duolink® In Situ PLA® Probe Anti-Rabbit MINUS	Merck	DUO92005
Duolink® In Situ Detection Reagents Red	Merck	DUO92008
NVP-AEW541	MedChem Express	HY-50866
Afatinib	MedChem Express	HY-10261
Complete EDTA-free Protease Inhibitor Cocktail	Roche	11836170001
PhosSTOP Phosphatase Inhibitors	Roche	04906837001

Table 3 (continued) | List of key resources

REAGENT or RESOURCE	SOURCE	IDENTIFIER
Puromycin	Sigma-Aldrich	P8833
EGFR Active human recombinant	Sigma-Aldrich	SRP0239
TRIzol	Thermo Fisher Scientifics	15596018
Chloroform	Sigma-Aldrich	32211
Experimental models: Cell lines		
SH-SY5Y (*H.sapiens*)	ATCC	CRL-2266
293 T (*H.sapiens*)	ATCC	CRL-3216
Recombinant DNA		
Please see Table S1 for a complete list of this study	N/A	N/A
Software and algorithms		
Zen Blue2.6	Zeiss	N/A
ImageJ	National Institutes of Health	https://imagej.nih.gov/ij/
BioRender	N/A	https://biorender.com/
Other		
ChemiDoc™ Imaging System	Bio-Rad	12003153
96-well dot-blot apparatus	Bio-Rad	170-6545
Polyvinylidene difluoride membrane	Millipore	IPVH85R
0.2 µm cellulose acetate membranes	Sterlitech	CA023001
SulfoLink™ Immobilization Kit for Peptides	Thermo Scientific	44999
KAPA SYBR FAST	KAPA Biosystems	KK4600
Maxima First Strand cDNA Synthesis Kit for RT-qPCR	Thermo Fisher Scientific	K1642

Following a period of three weeks, the previously primed mouse received two booster injections with the peptide KLH.

RNA purification and qRT-PCR

Total RNA from SH-SY5Y cells was extracted using TRIzol reagent (Thermo Fisher Scientifics). cDNA was synthesized using Maxima First Strand cDNA Synthesis (Thermo Fisher Scientific). qRT-PCR was performed on a BioRad CFX Connect Real-Time PCR Detection System. Each PCR reaction was performed in triplicate and repeated at least three times. All used primers are listed in Table S2.

Filter trap assay

The Triton-fractionation assay was performed as previously described in refs. 25,48. Cells were harvested and lysed with the filter trap lysis buffer (1% Triton X-100 in 1x PBS, pH 7.4) containing 1 mM PMSF and a Complete EDTA-free Protease Inhibitor Cocktail (Roche, Basel, Switzerland), followed by brief sonication. The protein concentration was determined by the Bio-Rad Protein Assay (Bio-Rad Laboratories, Hercules, CA, USA). Before filtering, the samples were diluted to a final concentration of 1 µg/ml with filter trap lysis buffer containing 1% sodium dodecyl sulfate (SDS). The samples were then filtered through a 0.2 µm nitrocellulose membrane, using a 96-well dot-blot apparatus (Bio-Rad Laboratories). Before filtration, the membranes were immersed in Rinse buffer (1% SDS in 1X PBS, pH 7.4). Filter dots were washed once with 0.05% TBST (150 mM NaCl, and 0.05% Tween 20, 20 mM Tris-HCl, pH 7.4). Proteins trapped by the filter were detected by immunostaining following the procedure of immunoblotting described below.

Cell fractionation analysis

Cell fractionation was conducted as previously described in ref. 29. SH-SY5Y cells expressing shDNAJB1, V5-tagged DNAJB1 wild-type (WT), and mutant DNAJB1 were harvested by washing twice with ice-cold PBS. Cells were lysed in 500 µL of Triton soluble buffer (150 mM NaCl, 20 mM Tris-HCl, pH 7.4, 1% Triton X-100, 0.5 µM EDTA, and 10 mM PMSF) supplemented with Complete EDTA-free Protease Inhibitor Cocktail (Roche), and the mixture was rotated at 4 °C for 1 h. Following incubation, the cell lysates were centrifuged at 21,500 × g for 10 min at 4 °C, and the supernatants were collected as Triton-soluble fractions. Insoluble fractions were obtained by resuspending the pellets in 400 µL of SDS-soluble buffer (150 mM NaCl, 20 mM Tris-HCl, pH 7.4, 1% Triton X-100, 2% SDS, 1% sodium deoxycholate, 1% NP-40, 0.5 µM EDTA, and 10 mM PMSF) containing Complete EDTA-free Protease Inhibitor Cocktail (Roche) and subjecting the mixture to sonication. Both soluble and insoluble fractions were subsequently analyzed by Western blotting using the appropriate antibodies. All used antibodies are listed in Table 3.

Duolink PLA

Based on the manufacturer's instruction (Duolink PLA, Merck), SH-SY5Y cells were transfected with empty vector, DNAJB1 WT, Y5F, or Y5E along with myc-tagged A53T α-synuclein, and seeded onto glass coverslips The coverslips were washed with ice-cold PBS, fixed with 4% paraformaldehyde for 10 min on the shaker, followed by a 5 min permeabilization process with 0.1% Triton x-100 (prepared in PBS) at room temperature. Subsequently, the cells were immersed in Duolink blocking solution for 1 h at 37 °C and then probed with primary antibodies overnight at 4 °C. The cells were incubated with Duolink PLA probes for 1 h at 37 °C after washing twice with Duolink Wash Buffer A. Afterward, the oligo ligation and fluorescence amplification were conducted using the Detection Reagents Red kit. The nuclear DNAs within the cells were stained with DAPI after washing the cells with Duolink Wash Buffer B. At last, the 25 coverslips were placed downward on slides and mounted with FluoromountTM Aqueous Mounting Medium overnight in a light-avoiding box. The nuclear DNAs within the cells were stained with DAPI after washing the cells with Duolink Wash Buffer B. At last, the coverslips were placed downward on slides and mounted with FluoromountTM Aqueous Mounting Medium overnight in a light-avoiding box.

Co-IP

1×10^6 SH-SY5Y cells were seeded in a 10-cm dish for 24 h, and 4 µg plasmids were transfected for 48 h. After 100 nM rotenone treatment for 24 h, cells were harvested and lysed in immunoprecipitation (IP) buffer (125 mM NaCl, 0.1% NP-40, 1 mM EDTA, 1 mM PMSF, 50 mM Tris–HCl pH 7.5, 10 mM NaF),

supplemented with Complete EDTA-free Protease Inhibitor Cocktail and PhosSTOP Phosphatase Inhibitors (Roche). Cell lysates (500 µg in 500 µl) were incubated 2.5 h with anti-V5 antibody (2 µg, #ab9916, Abcam) at 4 °C. Immunocomplexes were then isolated with protein G Mag Sepharose Xtra magnetic beads (Cytiva) for 2 h at 4 °C. After extensive washing with IP buffer three times, the bound proteins were eluted with 40 µl of 2x SDS sample buffer (250 mM Tris, pH 6.8, 10% SDS, 0.25% bromophenol blue, 50% sucrose, 0.5 M 2-mercaptoethanol). Precipitates were then analyzed by western blotting with appropriate antibodies. All used antibodies are listed in Table 3.

Western blotting

Whole proteins were extracted and resolved by SDS-polyacrylamide gel electrophoresis (SDS-PAGE) and transferred to a polyvinylidene difluoride membrane (PVDF) (Millipore). The membrane was blocked in 5% nonfat milk at room temperature for 1 h, followed by incubation with appropriate primary antibodies at 4 °C overnight. The primary antibodies are listed in the Reagents and Tools Table. After overnight incubation with the primary antibody, the membrane was washed three times with 0.05% TBST (150 mM NaCl, and 0.05% Tween 20, 20 mM Tris-HCl, pH 7.4). Next, the membrane was hybridized with the secondary anti-mouse and anti-rabbit peroxidase-conjugated antibodies from Jackson ImmunoResearch Inc. (West Grove, PA, USA). Signals were developed using LuminataTM Crescendo Western HRP Substrate (Millipore). The image was quantified by ImageJ software.

Immunofluorescence and confocal microscopy

7.5×10^4 cells were seeded onto glass coverslips (Marienfeld Laboratory Glassware, Germany) in 6-well plates and fixed with 4% paraformaldehyde in PBS for 15 min at room temperature. Fixed cells were washed with PBS and permeabilized with 0.1% Triton X-100 in PBS for 5 min. After washing three times with PBS, the cells on the coverslips were blocked in the 1% bovine serum albumin (BSA) for 0.5 h at room temperature. After blocking, the coverslips were incubated with EEA1 (1:200, 634169, GeneTex, USA), LAMP-1 (1:200, 14-1079-80, Invitrogen, USA), SQSTM1/P62 (1:200, 629890, GeneTex, USA), anti-V5 (1:100, 29137, GeneTex, USA) and anti-α-synuclein (1:250, 11279, Genetex, USA) specific antibodies overnight at 4 °C. The coverslips were incubated with AlexaFluor® 594 goat Anti-mouse IgG (H + L) (1:200, A11005, Invitrogen, USA), AlexaFluor® 488 chicken anti-goat IgG (H + L) (1:200, A21467, Invitrogen, USA) and Alexa Fluor™ 647 Goat anti-Rabbit IgG (H + L) (1:200, A21245, Invitrogen, USA) for 1 h at room temperature. After washing three times with PBS, the coverslips were stained with DAPI for 5 min, and cells were mounted with a mounting medium (Sigma, USA). Confocal images were captured under the Zeiss LSM780 confocal microscope.

E. coli recombinant protein purification

The fusion protein comprising DNAJB1 WT and DNAJB1 Y5F was expressed in BL21 (DE3) cells. A single colony was inoculated into 3 mL LB broth supplemented with 3 µL kanamycin and chloramphenicol (CM), and cultured overnight at 37 °C. Subsequently, 1 mL of the bacterial culture was transferred into 100 mL LB broth containing both antibiotics and incubated at 37 °C until the optical density at 600 nm (O.D.600) reached between 0.6 and 0.8. Induction with IPTG was performed at 16 °C overnight. Following induction, bacterial cells were harvested by centrifugation at 13,300 rpm for 5 min. The supernatant was discarded, and the cell pellet was resuspended and lysed in lysis buffer (0.1% NP40, 100 mM NaCl, 50 mM NaH_2PO_4, 10 mM imidazole, 10% glycerol, 1 mM PMSF, 3 mM 2-mercaptoethanol, pH 8.0) on ice for 1 h, followed by sonication for 2 min with 10-second intervals. The cleared lysate was then centrifuged at 12,000 g for 10 min to remove cell debris. The resulting supernatant was incubated with Talon His agarose beads (GE Healthcare) for 1 h at 4 °C, followed by two washes with wash buffer (100 mM NaCl, 50 mM NaH_2PO_4, 10 mM imidazole, 10% glycerol, 1 mM PMSF, pH 8.0). Finally, the fusion protein was eluted from the beads three times using His elution buffer (100 mM NaCl, 50 mM NaH_2PO_4, 500 mM imidazole, pH 8.0) and concentrated using Amicon Ultra Centrifugal Filters (3 kDa cutoff).

In vitro kinase assay

The EGFR kinase buffer contains 50 mM HEPES, 0.01% Tween-20, 10 mM $MnCl_2$, 10 mM $MgCl_2$, 1 mM EGTA, 2.5 mM DTT, and 0.1 mM ATP, pH 7.4. 1 µg purified recombinant WT or mutant DNAJB1 was incubated with 0.2 µg commercial EGFR (#SRP0239, Sigma. USA) in kinase buffer for 30 min at 30 °C. The kinase reaction was stopped in 5x SDS loading dye (5% 2-mercaptoethanol, 0.02% bromophenol blue, 30% glycerol, 10% SDS, and 250 mM Tris pH 6.8). The reaction was analyzed by Western blotting.

Quantification and statistical analysis

All experiments were performed with at least three biological repeats. Data were analyzed with Prism (Graph Pad, San Diego, USA). Paired data were expressed as mean ± standard deviation (SD) and analyzed using the student's t-test, one-way ANOVA with Dunnett's test, two-way ANOVA with Dunnett's test, and two-way ANOVA with Sidak's test. Statistical differences at $p < 0.05$ were considered significant. Further information about statistical tests, p values, and sample size are described in the figure legends.

Other information

The images of the full immunoblots are in Fig. S6.

Data availability

All data generated or analyzed during this study are included in this article.

Materials availability

All materials generated in this study are available from the corresponding authors with a complete Materials Transfer Agreement.

Received: 29 November 2024; Accepted: 21 May 2025;
Published online: 07 June 2025

References

1. Postuma, R. B. et al. MDS clinical diagnostic criteria for Parkinson's disease. *Mov. Disord.* **30**, 1591–1601 (2015).
2. Fearnley, J. M. & Lees, A. J. Ageing and Parkinson's disease: substantia nigra regional selectivity. *Brain* **114**, 2283–2301 (1991).
3. Braak, H. et al. Staging of brain pathology related to sporadic Parkinson's disease. *Neurobiol. Aging* **24**, 197–211 (2003).
4. Kalia, L. V. & Lang, A. E. Parkinson's disease. *Lancet* **386**, 896–912 (2015).
5. López-Otín, C., Blasco, M. A., Partridge, L., Serrano, M. & Kroemer, G. Hallmarks of aging: An expanding universe. *Cell* **186**, 243–278 (2023).
6. Hipp, M. S., Kasturi, P. & Hartl, F. U. The proteostasis network and its decline in ageing. *Nat. Rev. Mol. Cell Biol.* **20**, 421–435 (2019).
7. Kim, Y. E., Hipp, M. S., Bracher, A., Hayer-Hartl, M. & Hartl, F. U. Molecular chaperone functions in protein folding and proteostasis. *Annu Rev. Biochem* **82**, 323–355 (2013).
8. Hartl, F. U., Bracher, A. & Hayer-Hartl, M. Molecular chaperones in protein folding and proteostasis. *Nature* **475**, 324–332 (2011).
9. Chen, Y. C. et al. Glucose intake hampers PKA-regulated HSP90 chaperone activity. *Elife* **7**. https://doi.org/10.7554/eLife.39925 (2018).
10. Chen, H.-Y. et al. ATM-mediated co-chaperone DNAJB11 phosphorylation facilitates α-synuclein folding upon DNA double-stranded breaks. *NAR Mol. Med.* **1**, https://doi.org/10.1093/narmme/ugae007 (2024).
11. Mayer, M. P. & Bukau, B. Hsp70 chaperones: cellular functions and molecular mechanism. *Cell Mol. Life Sci.* **62**, 670–684 (2005).
12. Ayala Mariscal, S. M. & Kirstein, J. J-domain proteins interaction with neurodegenerative disease-related proteins. *Exp. Cell Res* **399**, 112491 (2021).
13. Nachman, E. et al. Disassembly of Tau fibrils by the human Hsp70 disaggregation machinery generates small seeding-competent species. *J. Biol. Chem.* **295**, 9676–9690 (2020).
14. Gao, X. et al. Human Hsp70 Disaggregase Reverses Parkinson's-Linked α-Synuclein Amyloid Fibrils. *Mol. Cell* **59**, 781–793 (2015).

15. Wentink, A. S. et al. Author Correction: Molecular dissection of amyloid disaggregation by human HSP70. *Nature* **589**, E2 (2021).
16. Schneider, M. M. et al. The Hsc70 disaggregation machinery removes monomer units directly from α-synuclein fibril ends. *Nat. Commun.* **12**, 5999 (2021).
17. Zarouchlioti, C., Parfitt, D. A., Li, W., Gittings, L. M. & Cheetham, M. E. DNAJ Proteins in neurodegeneration: essential and protective factors. *Philos. Trans. R Soc. Lond. B Biol. Sci.* **373**, https://doi.org/10.1098/rstb.2016.0534 (2018).
18. Deshayes, N., Arkan, S. & Hansen, C. The Molecular Chaperone DNAJB6, but Not DNAJB1, Suppresses the Seeded Aggregation of Alpha-Synuclein in Cells. *Int. J. Mol. Sci.* **20**, https://doi.org/10.3390/ijms20184495 (2019).
19. Saveri, P. et al. DNAJB2-related Charcot-Marie-Tooth disease type 2: Pathomechanism insights and phenotypic spectrum widening. *Eur. J. Neurol.* **29**, 2056–2065 (2022).
20. Sanchez, E. et al. Identification of a Large DNAJB2 Deletion in a Family with Spinal Muscular Atrophy and Parkinsonism. *Hum. Mutat.* **37**, 1180–1189 (2016).
21. Iwakura, Y. et al. Influences of dopaminergic lesion on epidermal growth factor-ErbB signals in Parkinson's disease and its model: neurotrophic implication in nigrostriatal neurons. *J. Neurochem* **93**, 974–983 (2005).
22. Jiang, Q. W. et al. Plasma epidermal growth factor decreased in the early stage of Parkinson's disease. *Aging Dis.* **6**, 168–173 (2015).
23. Qu, Y. et al. Estimated glomerular filtration rate is a biomarker of cognitive impairment in Parkinson's disease. *Front Aging Neurosci.* **15**, 1130833 (2023).
24. Jin, J. et al. Association between epidermal growth factor receptor gene polymorphisms and susceptibility to Parkinson's disease. *Neurosci. Lett.* **736**, 135273 (2020).
25. Chen, H. Y., Lin, C. H. & Teng, S. C. Stress-induced p53 drives BAG5 cochaperone expression to control α-synuclein aggregation in Parkinson's disease. *Aging (Albany NY)* **12**, 20702–20727 (2020).
26. Chang, Y. L. et al. The HSP40 family chaperone isoform DNAJB6b prevents neuronal cells from tau aggregation. *BMC Biol.* **21**, 293 (2023).
27. Chen, H. Y. et al. Clinical and functional characterization of a novel STUB1 frameshift mutation in autosomal dominant spinocerebellar ataxia type 48 (SCA48). *J. Biomed. Sci.* **28**, 65 (2021).
28. Chen, H. Y. et al. A novel C19orf12 frameshift mutation in a MPAN pedigree impairs mitochondrial function and connectivity leading to neurodegeneration. *Parkinsonism Relat. Disord.* **109**, 105353 (2023).
29. Wan, O. W. & Chung, K. K. The role of alpha-synuclein oligomerization and aggregation in cellular and animal models of Parkinson's disease. *PLoS One* **7**, e38545 (2012).
30. Boer, D. E. C., van Smeden, J., Bouwstra, J. A. & Aerts, J. Glucocerebrosidase: Functions in and Beyond the Lysosome. *J. Clin. Med.* **9**, https://doi.org/10.3390/jcm9030736 (2020).
31. Sidransky, E. et al. Multicenter analysis of glucocerebrosidase mutations in Parkinson's disease. *N. Engl. J. Med* **361**, 1651–1661 (2009).
32. Stojkovska, I. et al. Rescue of α-synuclein aggregation in Parkinson's patient neurons by synergistic enhancement of ER proteostasis and protein trafficking. *Neuron* **110**, 436–451.e411 (2022).
33. Rosety, I. et al. Impaired neuron differentiation in GBA-associated Parkinson's disease is linked to cell cycle defects in organoids. *NPJ Parkinsons Dis.* **9**, 166 (2023).
34. Eom, J. W., Lee, J. Y., Kwon, Y. & Kim, Y. H. An increase of lysosomes through EGF-triggered endocytosis attenuated zinc-mediated lysosomal membrane permeabilization and neuronal cell death. *Cell Death Dis.* **15**, 823 (2024).
35. Kohler, V. & Andréasson, C. Hsp70-mediated quality control: should I stay or should I go?. *Biol. Chem.* **401**, 1233–1248 (2020).
36. Rosenzweig, R., Nillegoda, N. B., Mayer, M. P. & Bukau, B. The Hsp70 chaperone network. *Nat. Rev. Mol. Cell Biol.* **20**, 665–680 (2019).
37. Zuiderweg, E. R., Hightower, L. E. & Gestwicki, J. E. The remarkable multivalency of the Hsp70 chaperones. *Cell Stress Chaperones* **22**, 173–189 (2017).
38. Tanzi, R. E. The genetics of Alzheimer disease. *Cold Spring Harb. Perspect. Med.* **2**, https://doi.org/10.1101/cshperspect.a006296 (2012).
39. Klein, C. & Westenberger, A. Genetics of Parkinson's disease. *Cold Spring Harb. Perspect. Med* **2**, a008888 (2012).
40. Tsalenchuk, M., Gentleman, S. M. & Marzi, S. J. Linking environmental risk factors with epigenetic mechanisms in Parkinson's disease. *NPJ Parkinsons Dis.* **9**, 123 (2023).
41. Park, S. Y. et al. DNAJB1 negatively regulates MIG6 to promote epidermal growth factor receptor signaling. *Biochim Biophys. Acta* **1853**, 2722–2730 (2015).
42. Leong, Y. Q., Koh, R. Y., Chye, S. M. & Ng, K. Y. Unravelling the genetic links between Parkinson's disease and lung cancer. *Biol. Chem.* **404**, 551–567 (2023).
43. Møller, H., Mellemkjaer, L., McLaughlin, J. K. & Olsen, J. H. Occurrence of different cancers in patients with Parkinson's disease. *Bmj* **310**, 1500–1501 (1995).
44. Ajdacic-Gross, V. et al. Cancer co-occurrence patterns in Parkinson's disease and multiple sclerosis-Do they mirror immune system imbalances?. *Cancer Epidemiol.* **44**, 167–173 (2016).
45. Park, J. H. et al. Cancer risk in patients with Parkinson's disease in South Korea: A nationwide, population-based cohort study. *Eur. J. Cancer* **117**, 5–13 (2019).
46. Lebovitz, C. et al. Loss of Parkinson's susceptibility gene LRRK2 promotes carcinogen-induced lung tumorigenesis. *Sci. Rep.* **11**, 2097 (2021).
47. Yan, Y. et al. SNCA Is a Functionally Low-Expressed Gene in Lung Adenocarcinoma. *Genes.* (Basel) **9**, https://doi.org/10.3390/genes9010016 (2018).
48. Xu, G., Gonzales, V. & Borchelt, D. R. Rapid detection of protein aggregates in the brains of Alzheimer patients and transgenic mouse models of amyloidosis. *Alzheimer Dis. Assoc. Disord.* **16**, 191–195 (2002).

Acknowledgements

We thank the Image Core Facility of NTU for the technical support of immunofluorescence staining. The study was funded by the National Science and Technology Council in Taiwan [112-2311-B-002 -015 -MY3] to S.-C. Teng and National Health Research Institutes [NHRI-EX113-11136NI] to C.-H. Lin.

Author contributions

S.-C.T. designed the research. S.-J.L., C.-Y.L., Y.-T.C, and Y.-L C. prepared the experimental materials. Y.-Y.H., C.-C.Y., W.-Y.C. and C.-Y.L. collected the data. Y.-Y.H. analyzed the data. Y.-Y.H. and S.-C.T. wrote the manuscript with the help of C.-H.L. All authors performed experiments mentioned in the paper. All authors read and approved the final manuscript.

Competing interests

The authors declare no competing interests.

Additional information

Supplementary information The online version contains supplementary material available at https://doi.org/10.1038/s41531-025-01006-y.

Correspondence and requests for materials should be addressed to Chin-Hsien Lin or Shu-Chun Teng.